ORIGINAL ARTICLE

Thermomechanical analysis of riveted carbon fiber laminates for aerospace applications

Gennaro Scarselli [ID] | Stefano Carrino | Riccardo Nobile

Department of Engineering for Innovation, University of Salento, Lecce, Italy

Correspondence
Gennaro Scarselli, Department of Engineering for Innovation, University of Salento, Via per Monteroni, 73100 Lecce, Italy.
Email: gennaro.scarselli@unisalento.it

Abstract

Experimental fatigue tests performed on riveted carbon fiber laminates showed that the specimens, after some thousands of cycles, heated up, reaching around the rivet holes high temperatures. These temperatures if not properly controlled could be detrimental for the joint health. In order to understand the relative importance of all the mechanical and geometric parameters involved in the joint manufacturing, a numerical model of the joined carbon fiber laminates was developed using a commercial finite elements code. A simplified analytical model of heat transfer was then used to simulate the rivets thermal behavior under the assigned operating conditions: this model allowed comparisons with finite elements and can be used for simple thermal simulations. The numerical and analytical results were found in a good agreement with the available experimental results. The present research conclusions can be used for drawing better design rules in the definition of riveted carbon fiber laminates.

KEYWORDS
fatigue, finite element analysis (FEA), laminates, thermomechanics

1 | INTRODUCTION

Carbon fiber-reinforced plastics (CFRP) structures are widely used in aeronautic field in order to improve resistance/weight ratios and to reduce fuel consumption. Although the principal limits are well known for any loading conditions, particular care and attention are required in the case of material junctions as in the case of mechanical fastener employment. Useful review papers[1–3] introduce the reader to a better comprehension of the phenomena involved in determining mechanical behavior of fastened joints. Nevertheless, its complexity, stress field around a pin-loaded hole has been largely studied considering the effect of friction, clearance, contact, and geometrical parameters.[4–12] Static behavior of mechanically fastened joints could be well determined through an experimental test campaign following, for example, ASTM standards.[13,14] The application of a fatigue load changes significantly this behavior. Fatigue behavior of bearing specimen could be determined through experimental test following ASTM D6873.[15] The mechanical behavior of bolted joints subjected to in-plane tensile loads until the failure is described by a three-dimensional progressive damage model by Tserpes et al.[16] Local slippage phenomena due to uncertainty of laminate and bolt joint are particularly important in dynamic loading. If a fatigue load is applied and the load level is higher than the maximum friction load, a slipping of the surface is originated at each load reversal. This determines several detrimental phenomena concerning the load transmissibility capacity of the joint consisting in hole wear, damage of contact surfaces between the

composite parts, and growth of delamination starting from the hole.[17] As a consequence, initial prestress induced by rivets could influence fatigue behavior, as observed in other works.[18–21]

Another aspect of the fatigue behavior of bolted joint is represented by the thermomechanical equilibrium of the joint subjected to variable loads. The slippage and friction between laminates determine at each cycle dissipative phenomena, which causes a temperature increase of the joint. Few works considered the effect of elevated temperature on the fatigue behavior of bolted joints: generally, experimental fatigue tests of bolted joints are carried out varying and limiting the frequency in order to limit the maximum temperature of bolts to 33°C.[22] Counts and Johnson[23] reported the experimental behavior of fatigue tests carried out at 177°C observing in particular that the fatigue results were insensitive to frequency variation in the range 0.1–10 Hz. However, in this case, temperature test was so different from room temperature that the local heating of bolts induced by fatigue load would be negligible with respect to the thermal energy exchanged with the surrounding ambient.

More interesting is the methodology reported in other works[24,25] in which experimental tests at a temperature of 90°C were carried out. In this case, the authors recognized that the temperature increase induced by fatigue loading could be relevant in determining the damage evolution of the joint. The temperature variation of the joint was assumed to be proportional to the number of cycles to failure N_f and the square of the stress range $\Delta\sigma$. The authors followed in this case the suggestion of Sauer and Richardson[26] that indicated that thermal energy dissipation under fatigue is proportional to the square of stress amplitude and load cycle frequency. However, the proposed model was based on a phenomenological approach, trying to describe the global effect without considering the mutual influence of the parameters on the thermomechanical behavior of the joint. Moreover, tests were carried out at higher level of temperature with respect to room temperature conditions, and this circumstance mitigated the thermal effect on the fatigue performance.

These limitations and simplifications have been overcome in the present work in which the main novelty consists in a deep analysis of all the factors that influence the thermomechanical behavior of a bolted joint subjected to fatigue loading. All the experimental and numerical indications have been used to develop a simplified thermomechanical model able to describe the behavior of bolted joints under fatigue loading. The finite element (FE) model considers not only the usual parameter of applied stress, frequency, and nominal geometry of the joint but also the variability of the technological parameters that affects normally the resulting joint, as for example the effective values of geometrical parameters and the effective clamping loads originated by the rivets mounting. The numerical model developed in this work is able to describe accurately the results of an experimental test campaign carried out on single lap riveted joints by the authors.[27,28] The second important result of this paper is that the thermomechanical behavior of a riveted joint subjected to fatigue loads could be simply and globally described analytically as a first-order system, if the characteristic time constant is determinable and provided that the thermal load is evaluated numerically. Eventually, the authors give the indication to determine this fundamental time constant starting from the knowledge of the main parameters that describe the fatigue load that are as follows: applied stress range, frequency, and specific combination of geometrical parameters.

2 | MATERIALS AND METHODS

2.1 | Specimens' materials and geometry

Specimens were manufactured using a 16-plies symmetric carbon/epoxy laminate made from unidirectional prepregs (commercial name IMS 977-2) following a standard prepreg lay-up process. The stacking sequence was $[45,0,-45,90]_2s$ so the laminates were defined "angle-ply" with the fiber directions out of the principal axis. After the cure process in autoclave, the laminate was cut to obtain the doublers and the two parts A and B forming the specimen. Eventually, holes were obtained through a high-speed drilling process in order to reduce the material damage. The used carbon fibers had an intermediate modulus of elasticity (IM, $290\,GPa$) and density of $1.785\,\frac{g}{c}m^3$ with a linear density of 830 tex $\left(\frac{g}{km}\right)$.

The resin used for the prepreg was the epoxy CYCOM 977-2, with a curing temperature of 177°C, with a 170°C dry and 135°C wet glass transition temperatures, formulated for autoclave or press molding manufacturing. The epoxy resin had an elasticity modulus of $3.65\,GPa$ and a density of $1.31\,\frac{g}{c}m^3$. From the Classic Laminate Theory (CLT), micromechanics and macromechanics, the global

TABLE 1 Mechanical properties of the laminate

Thickness (mm)	3.0	G_{yz} (GPa)	3.75
Density (g/cm^3)	1.62	ν_{xy}	0.317
E_x (GPa)	64.6	ν_{xz}	0.269
E_y (GPa)	64.6	ν_{yz}	0.269
E_z (GPa)	9.67	ν_{yx}	0.317
E_{xy} (GPa)	24.5	ν_{zx}	0.0403
E_{xz} (GPa)	3.75	ν_{zy}	0.0403

mechanical properties of laminate were calculated and are reported in Table 1. The single-body modeled rivets were made of Ti-6Al-4V titanium alloy with a density of 4.43 $\frac{g}{c}m^3$ and an elasticity modulus of 113.8 GPa. The doublers were made of the same material of laminates. The laminate mechanical properties were obtained by homogenization, exploiting a composite design tool, in-house developed, that quickly provides simulation information about composite materials, laminates, and simple structures.

The specimen under exam is a single lap joint made of two laminated plates joined by two Hi-Lok rivets having a nominal diameter of 6.35 mm. Specimen geometry follows the indications of the ASTM standard (Figure 1) relevant for the specific fatigue test to be performed: the laminates, with a length of 210 mm and a width of 38.1 mm, have a constant rectangular cross-section 3 mm thick. The bolt holes have a nominal diameter of 6.35 mm and a distance from each other equal to four times the diameter. The overlapping region has a total length of 63.5 mm equal to 10 rivets diameters. The doublers bonded at the end of each laminate have a length of 121 mm.

The geometrical configuration of the single lap joint has been reproduced in an FE model: due to the symmetric load conditions and geometry, only one half of the joint was modeled imposing proper boundary conditions on the symmetry plane. The joint behavior is affected by the clearance arising from the difference between hole and fastener diameters. To evaluate the influence of this clearance on the static and dynamic specimen response, three different geometries characterized by three different sliding distances (Figure 1) were considered in addition to the nominal one. The detail of the geometrical values that define the three configurations of interest is reported in Table 2. The geometry was modeled by Design Modeler,[29] a CAD software integrated in Ansys Workbench.

2.2 | Numerical simulations

FE models were developed using the commercial code Ansys Workbench to simulate the heating generation and the thermal propagation through the joint components under the action of fatigue cycle loads. The first step of the procedure is the "Static Structural Analysis" aimed at defining a FE model able to describe the actual structural behavior experimentally tested before.[27,28] From this analysis, the sliding load was evaluated to identify the condition leading to the *rubbing* of the two plates useful to simulate the fatigue cyclic tests. The second step is the "Transient Thermo-Structural Analysis" that provides the thermal loads generated at each cycle. The third step is the "Transient Thermal Analysis" based on the application of the thermal loads previously
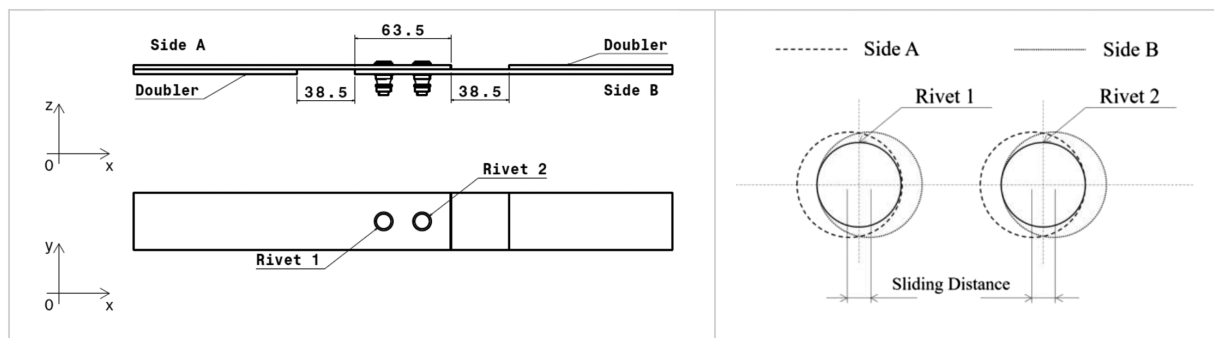

FIGURE 1 Specimen geometry

TABLE 2 Definition of the geometrical configuration of the joint (the tolerance on the hole diameter is ±0.76 mm; the tolerance on the rivet diameter is ±0.013 mm)

	Side A		Side B				
	Hole 1 (mm)	Hole 2 (mm)	Hole 1 (mm)	Hole 2 (mm)	Rivet 1 (mm)	Rivet 2 (mm)	Sliding distance (mm)
Configuration 1	6.35	6.35	6.35	6.35	6.330	6.330	0.040
Configuration 2	6.35	6.35	6.35	6.35	6.250	6.250	0.200
Configuration 3	6.35	6.35	6.35	6.35	6.160	6.160	0.380

evaluated in order to estimate the temperature field after an assigned number of fatigue cyclic tests.

2.3 | Mesh

In the finite element method (FEM), mesh density is a significant parameter used to control the results accuracy. A selective refinement is necessary in the region where considerable stress gradients and peaks caused by applied loads are present. In this case, the hole region is characterized by highly dense grid with smaller element size compared to those utilized in the far regions. There are various possibilities for the simulation of the tightening torque that can be present in the assembly of both rivets and bolts. The choice of the elements and the representation mode is determined by the degree of the desired complexity.[30] Riveted joint can be seen as the simultaneous action of three distinct parts: collar, pin, and washer. By tightening the collar on the pin of the bolt, the preload is generated that helps in holding together the different parts of the joint when they are subjected to forces trying to separate them. Pretension elements (PRETS179) were used to define a 2-D pretension section with only translational degree of freedom along the defined pretension direction. The pretension section was meshed by PSMESH command that subdivides rivet domain into two distinct meshes according to the definition of the preload direction and separated at two initially coincident surfaces. The value of pretension

load is calculated as a function of the tightening torque applied to the collar:

$$P = \frac{T}{k_T \, d_{PIN}}, \tag{1}$$

where P is the preload, T the applied tightening torque, d_PIN the pin diameter, and k_T the torsion coefficient assumed equal to 0.2.[30] Three different values of the tightening torque are used: 1.975, 3.95, and 7.9 Nm.

3 | EXPERIMENTAL RESULTS

Several tests on riveted single-lap joints (SLJs) made of carbon/epoxy laminates were carried out with different frequencies and load levels.[27] However, fatigue tests were characterized by triangular load cycles and load ratio $R = -1$. The load was applied in the direction of the joint (x-axis) by using a metallic support fixture to avoid buckling phenomena during compression. The support fixture was modeled by imposing zero displacement on the areas highlighted in Figure 2. Negative values of load ratio R resulted in vanishing the clearance between holes and fasteners generating significant temperature increases for the combination of slipping and friction at the laminates interface. This condition is the most dangerous and critical because the load inversion causes a slippage equal to the total hole clearance for each cycle with a consequent notable amount of heat produced at the laminates interface.
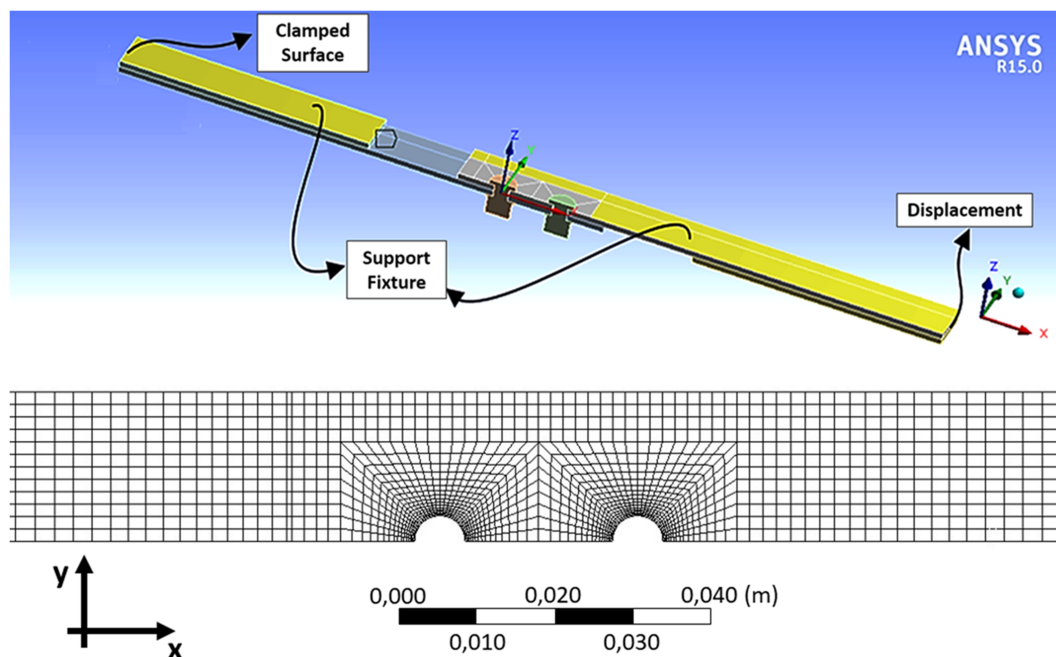

FIGURE 2 Finite element (FE) model of the specimen [Colour figure can be viewed at wileyonlinelibrary.com]

These phenomena became considerably relevant at higher frequency and load levels, as observed by the authors[27] where fatigue test results are reported. As a consequence, the fatigue behavior of the joint was found very sensitive to the clearance existing between hole and rivets. The authors decided to monitor the temperature field around the holes by using an infrared (IR) camera TVS-600 Avio as shown in Figure 3. In the region between the two rivets, considerable increments of temperature are observable with high temperature gradients nearby the rivet holes.

The temperature maps around the fasteners were obtained by postprocessing in Matlab the IR camera data at different cycles for three experimental cases of interest, which differs for frequency, applied load, and geometrical configuration according to Tables 2 and 3. The combination of these three parameters, in particular the controllable ones of frequency and applied load, resulted in a different amount of thermal energy dissipation according to the observations of Sauer and Richardson.[26] In this manner, the three tests covered with good approximation all the effective conditions of the specimens and constituted an experimental basis for the verification of the analytical model proposed in this paper. The temperature evolution during the fatigue test is clearly showed in Figure 4, in which the isothermal lines obtained through filtering and elaboration of thermal data are superimposed to the detail of the joint at different number of cycles.

4 | DISCUSSION OF RESULTS

In the following three subsections, the discussion of the results is provided: initially, the static analyses obtained from the finite element models of the joint are discussed;

subsequently, the thermal transient analyses simulating the fatigue tests are detailed with a particular focus on the generated thermal power; then, an analytical model of the riveted joint is introduced; eventually, the experimental, numerical, and analytical correlation is carried out.

4.1 | Static structural analyses

For the static structural analysis, SOLID186 and SOLID187 elements with quadratic displacement were used to mesh, respectively, laminates and rivets allowing to obtain lower errors at the same number of used elements (p-refinement).[31] The presence in an assembly of contact zones results in nonlinearity of the structural response, both static and dynamic. Contacts are detected between two surfaces, one of which must be designated as the *contact* and the other one as the *target* and are modeled with three-dimensional CONTA174 and TARGE170 elements, respectively.[31] From the results of this analysis, it is possible to obtain the parameters needed for the definition of the bearing stress/bearing strain curve from which the joint stiffness was derived and the load value at which sliding between the two plates occurs was evaluated. The bearing stress was calculated as follow:

TABLE 3 Definition of the three experimental cases

	Geometry	Frequency (Hz)	Load (kN)
Case 1	Configuration 1	3.5	10
Case 2	Configuration 2	5	7.5
Case 3	Configuration 3	5	5

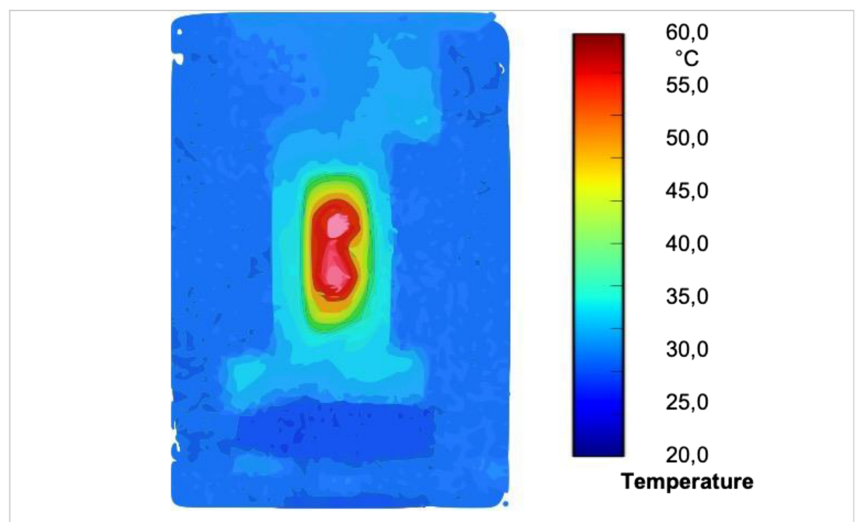**FIGURE 3** Temperature map around the rivets [Colour figure can be viewed at wileyonlinelibrary.com]
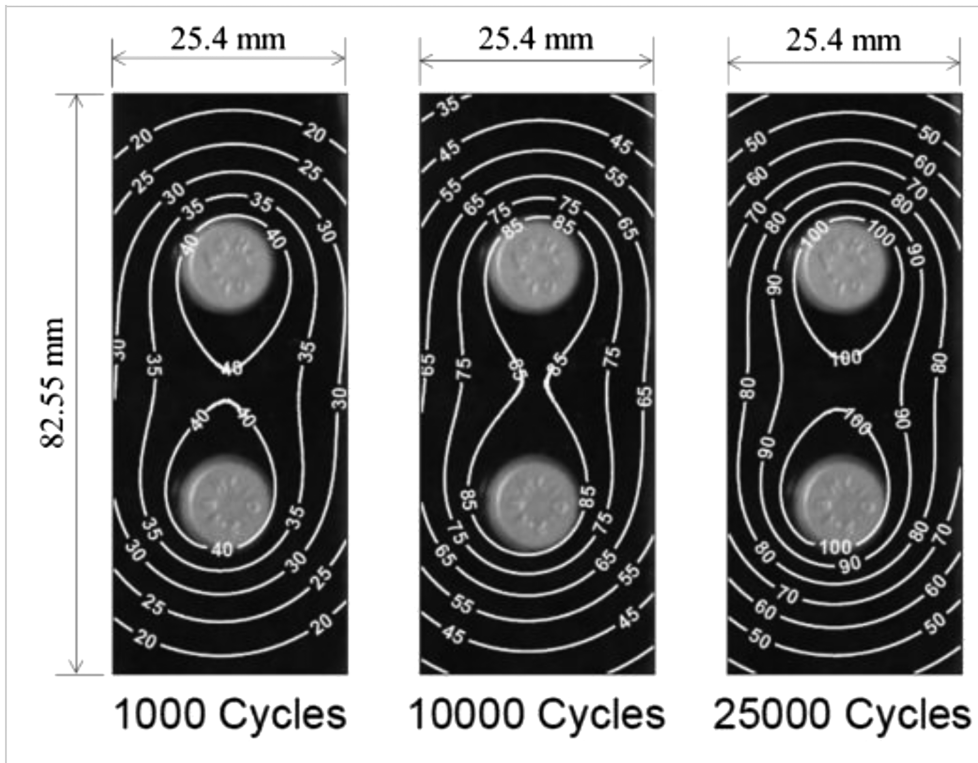
FIGURE 4 Configuration 2, load frequency = 5 Hz, load amplitude = 7.5 kN, T (°C)
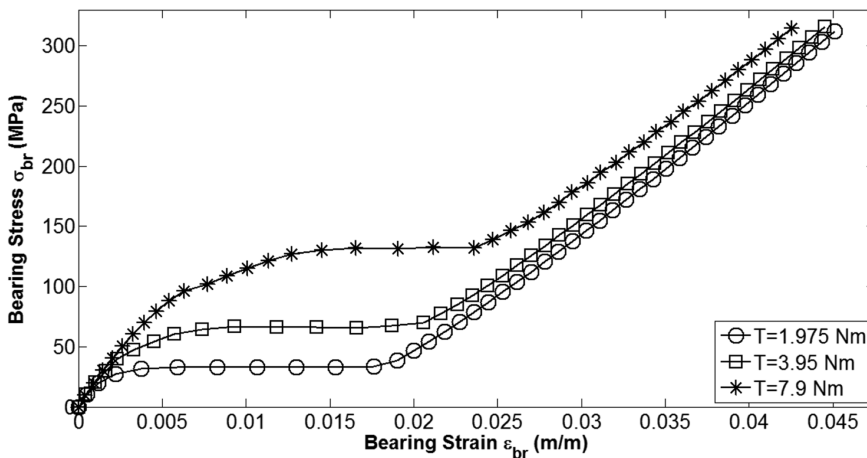

FIGURE 5 Configuration 2 ($f = 0.2$)

$$\sigma^{br} = \frac{k_b R_x}{hD}, \qquad (2)$$

$$\varepsilon^{br} = \frac{\delta_x^{side-B} - \delta_x^{side-A}}{D}. \qquad (3)$$

where k_b is a factor representing the amount of bearing deformation for each plate (a value of 0.5 was assumed meaning that each plate experiences half of the total deformation), R_x is the x-component of the reaction force resulting at the fixed support, h is the specimen thickness, and D is the hole diameter. The bearing strain was calculated as the ratio between the relative displacement δ_x of two points (belonging to laminates A and B; see Figure 1) and hole diameter:

In the structural analyses, a parametric study was carried out considering the three geometrical configurations reported in Table 1 in order to determine the joint stiffness and the sliding load varying the friction coefficient f (0.1, 0.15, and 0.2) and the tightening torque (1.975, 3.95, and 7.9 Nm). The experimental test carried out on eight specimens[27,28] showed a bearing stiffness falling in the range between 11.6 and 13.92 GPa. The FE model based on the nominal geometry provided a value for the

stiffness of 12.62 GPa while the parametric study on the three configurations provided values of stiffness between 11.07 and 12.45 GPa (Figures 5 and 6). This can be interpreted in the following way: bearing stiffness, ratio of applied stress to specimen elongation or slope of the bearing stress/bearing strain curve, is strongly depending on the joint clearance and decreases with it. At the same applied load, higher clearances result in smaller contact regions between rivets and holes: consequently, bearing stresses increase locally since the same applied force is distributed over a smaller area. This results in higher specimen elongations and then in smaller bearing stiffness. The following conclusions can be drawn:

1. For each configuration and for each value of the involved parameters, the bearing stress/bearing strain

curve shows a specific common behavior: on each curve, it is possible to identify five different regions that are reported only on Figure 6 for sake of brevity. At first, the pattern is linear (region I) with a slope that is almost the same for the different configurations (E'). Then a transition region (II) exists where the sliding between the two laminates starts, characterized by a variable decreasing slope and, eventually, by a zero slope. In this flat region (zero stiffness, III), the load is constant and the strain increases without any additional load. When the sliding is completed, the slope (joint stiffness) quickly increases again (there is a new transition region, IV) reaching values (E'' in region V) that are reported in Table 4; for Configuration 1, the flat region is barely visible with respect to Configurations 2 and 3: this is due to the different values of the
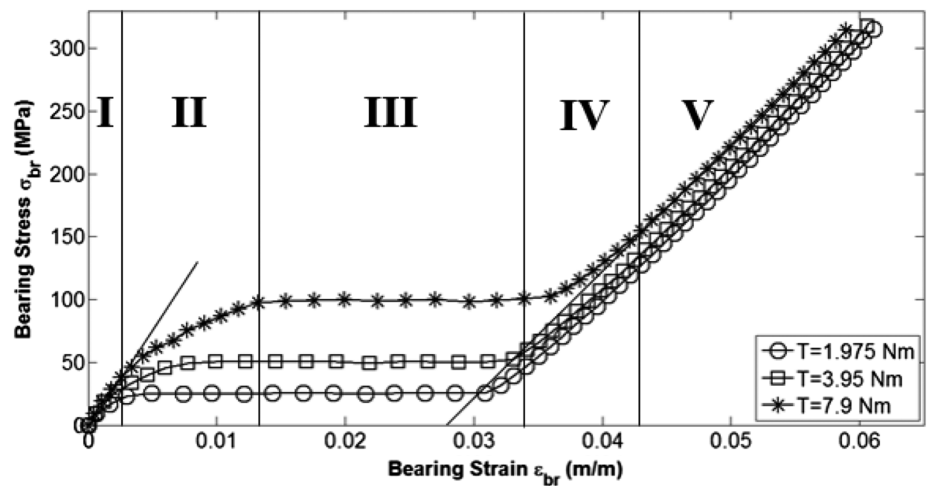

FIGURE 6 Configuration 3 ($f = 0.1$)

TABLE 4 Joint stiffness for the different configurations

Configuration 1

T (nm)	1.975	3.95	7.9	1.975	3.95	7.9	1.975	3.95	7.9
f	0.1	0.1	0.1	0.15	0.15	0.15	0.2	0.2	0.2
E' (MPa)	14,320	14,103	14,742	17,471	17,520	17,439	19,681	19,959	20,722
E'' (MPa)	12,641	12,444	12,449	12,449	12,476	12,459	12,559	12,502	12,451

Configuration 2

T (Nm)	1.975	3.95	7.9	1.975	3.95	7.9	1.975	3.95	7.9
f	0.1	0.1	0.1	0.15	0.15	0.15	0.2	0.2	0.2
E' (MPa)	14,302	14,108	15,522	17,445	17,483	18,721	19,648	19,918	20,733
E'' (MPa)	11,762	11,790	11,731	11,804	11,736	11,721	11,687	11,804	11,736

Configuration 3

T (Nm)	1.975	3.95	7.9	1.975	3.95	7.9	1.975	3.95	7.9
f	0.1	0.1	0.1	0.15	0.15	0.15	0.2	0.2	0.2
E' (MPa)	14,355	14,592	15,538	17,470	17,493	18,756	19,706	19,934	20,750
E'' (MPa)	11,108	11,155	11,133	11,212	11,086	11,100	11,254	11,158	11,067

sliding distance. For Configurations 2 and 3, the flat region is clearly visible in the curve and more extended for Configuration 3 characterized by a bigger sliding distance.

2. The transition region is more pronounced for big values of T while for small values of T sliding quickly occurs. This effect can be explained in the following way (see Figure 6): high values of T result in higher "sliding loads", that is, the applied loads at which the two laminates forming the joint slide on each other without a further increase of load. The transition region is more extended for big values of T since higher values of tightening torque result in higher stresses normal to laminate faces in contact and this counteracts the sliding of the two laminates.

3. According to the theory, the sliding load is a linear function of both friction coefficient and tightening torque: this is reasonable since higher friction coefficient values and higher tightening torque prevent the movement of the two laminates. The biggest sliding load was calculated for $f = 0.2$ and $T = 7.9$ Nm: in this case, a force of 3.8 kN caused the relative motion of the joined parts. The smallest value of sliding load 0.48 kN was obtained for $f = 0.1$ and $T = 1.975$ Nm.

4. The joint stiffness before the transition E' (see Table 4) slightly increases with the tightening torque T; on the other hand, E' is strongly affected by the friction coefficient: doubling the value of f from 0.1 to 0.2 results in an increase for E' of nearly 40%, and this can be explained since a bigger friction results in a stiffer joint: the contact points belonging to the two laminates are prevented in the relative movement by the friction force, and this results in an additional apparent stiffness.

5. The joint stiffness after the last transition E'' is smaller than E' and seems not to be affected by friction and tightening torque and for each configuration is nearly constant; E'' is affected instead by the sliding distance and decreases increasing this distance. The explanation of this effect comes from the same consideration reported before concerning the dependence of bearing stiffness on the clearance: increasing the clearance the applied load is distributed over a smaller area between rivet and hole resulting in a higher stress. Higher stress results in higher deformation and, consequently, in smaller bearing stiffness. The independence of E'' on friction and tightening force, instead, can be explained since in the region V, the sliding distance has been covered and rivets and holes are in close contact without any chance for the laminates to slide on each other.

4.2 | Transient thermostructural analysis

The purpose of thermostructural analysis was to calculate the heat generated by friction between the joined parts. Therefore, it was necessary to couple the structural and thermal degrees of freedom of the FE model. Since the aim of this phase of the work was to obtain the heat generated by the friction between the contact surfaces, the problem required specific attention to the contact areas. The simulation of slippage between the surfaces in this part of the work was always based on the use of the CONTA174 elements for which the nodal temperature was activated.[32] The following hypotheses are made on the finite element model: the energy developed by the friction between the joined laminates is entirely dissipated and transformed in thermal energy (conservative hypothesis); the whole heat flux generated is absorbed entirely by the bolt (conservative hypothesis); the heat propagates from the bolt to the laminates by thermal conduction. The amount of heat generated by dissipation was calculated as

$$q = FGTH * \tau_{ij} * V \ \left[\text{W/m}^2\right]. \tag{4}$$

FGTH is the frictional dissipated energy converted into heat, τ_{ij} is the equivalent shear stress ($[\frac{N}{m^2}]$) in the contact area and V the sliding rate ($[\frac{m}{s}]$). *FGTH* was assumed equal to 1 so all frictional energy is converted into heat. The amount of heat on *contact* and *target* surfaces is defined by

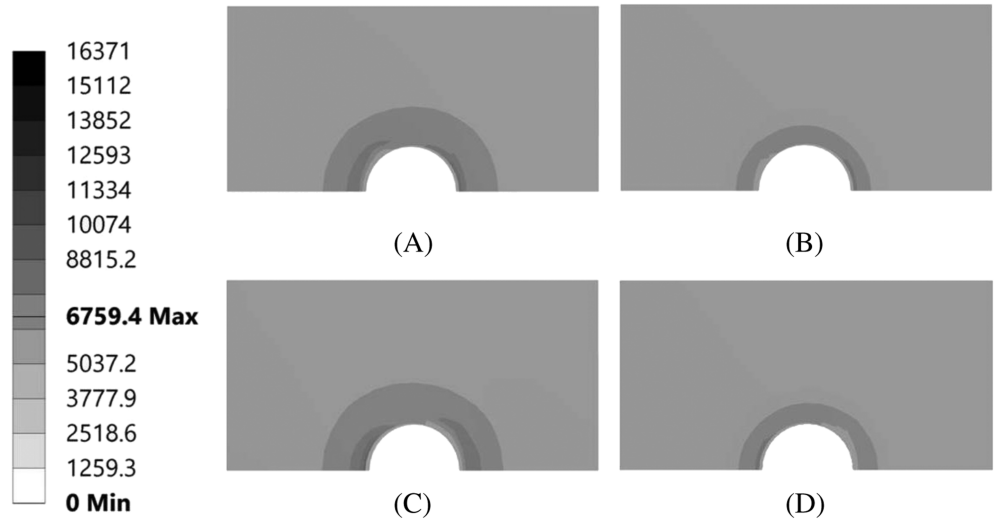$$q_c = FWGT * FGTH * \tau_{ij} * V \ \left[\text{W/m}^2\right], \tag{5}$$

$$q_T = (1 - FWGT) * FGTH * \tau_{ij} * V \ \left[\text{W/m}^2\right], \tag{6}$$

where q_c is the heat on the *contact area* and q_T is that on the *target area*. *FWGT* is the weight factor for the distribution of heat between the *contact* and *target* surfaces. In this case, *FWGT* was set equal to 0.5 because the parts joined are made up of the same material.[31] The constraint conditions of fatigue tests were the same of the static structural analysis. The model was subjected to a triangular cyclic load with a stress ratio R equal to -1 at different frequencies (2, 3.5, and 5 Hz) and amplitudes (5, 7.5, and 10 kN). The initial temperature was set at $22°C$. The simulations allowed to get the heat generated by friction after each load cycle (Figure 7) for the different cases of interest: as expected, the highest values of heat flux involved the model's elements that were located closest to the fastener region where more pronounced was the

D: Transient Structural
Generated Heat (Joule per square meter)
Expression: CONTSFRI*CONTSLID

16371
15112
13852
12593
11334
10074
8815.2

6759.4 Max

5037.2
3777.9
2518.6
1259.3
0 Min

(A)   (B)

(C)   (D)

effect of the pretension load due to tightening of the rivets.

4.3 | Analytical model for heat transfer

The specimen model, after the evaluation of the heat generated by the friction presented and discussed in Section 4.2, was then subjected only to the thermal loads acting at the interfaces of contact areas. Since this was a *purely thermal* problem, elements with nodal temperature as degree of freedom were used. Laminates and doublers were modeled with elements SOLID90 and the rivets with elements SOLID87. Unlike previous analyses, the contact nodes were considered bonded in order to remove thermal resistance and discontinuities of temperature arising at the interface and thus to generate perfect thermal coupling. This problem is governed by the thermal contact conductance (TCC) that is defined as

$$TCC = \frac{k_{xx}}{f_g}, \qquad (7)$$

where k_x is the highest thermal conductance among those of the used materials and f_g is a geometric factor that takes into account the overall model.[31] At the specimen walls not in contact with the metallic support (the fixture used for the experimental fatigue tests), a convection condition was applied imposing a convection coefficient h_f equal to $5.1 \frac{W}{m^2 \circ C}$ (result of a fitting process between experiments and numerical models) and a room

temperature $\vartheta_R T$ of $22°C$, respectively. The convection on these areas can be expressed as

$$q = h_f * \left(\vartheta_{surf} - \vartheta_{RT} \right), \qquad (8)$$

where $\vartheta_s urf$ was the surface temperature of these specimen walls. Thus, it was possible to calculate the number of cycles and loops according to the pre-set simulation time (i.e., the time duration of the simulated part of fatigue test assumed equal to $5000 s$). In this way $5000 s$ of fatigue test requested the running of 10,000, 17,500, and 25,000 $cyc \leq s$ for the analysis at 2.0, 3.5, and 5.0 Hz, respectively. The thermal state of the specimen was monitored through the temperature evaluated at the rivets. After these FE thermal analyses, an analytical model was developed to describe the rivets' heating. The simulated thermal phenomenon is the result of an interaction between conduction in the laminates and convection at its surface in contact with the ambient. Biot number (Bi) is a dimensionless number that gives an indication of the relative importance of conduction and convection in determining the temperature history of a body being heated.[33]

$$Bi = \frac{h_f L_c}{k} = \frac{\left(\frac{L_c}{k A_s} \right)}{\left(\frac{1}{h_f A_s} \right)} = \frac{\text{Conduction Thermal Resistence}}{\text{Convection Thermal Resistence}}.$$

$$(9)$$

In 9, A_s is convection area ($3.03 \cdot 10^{-4} m^2$), k thermal conductivity ($80.5 W m^{-1} \circ C^{-1}$), and L_c a characteristic

length calculated as the ratio between rivet volume V_r and A_s. Transient conduction problems with $Bi < 0.1$ may be treated simply as lumped parameter problem.[33] Titanium alloys (rivets materials) are characterized by a high thermal conductivity so Bi is equal to 1.25×10^{-4}. The rivets temperature was therefore assumed spatially uniform and function of time only.

The problem can be described by the following equations:

$$mc_p \vartheta(t)' = W - h_f A_s [\vartheta(t) - \vartheta_{RT}], \qquad (10)$$

$$\vartheta(t)' + \frac{hA_s}{mc_p} \vartheta(t) = \frac{W}{mc_p} + \frac{h_f A_s}{mc_p} \vartheta_{RT}, \qquad (11)$$

$$\vartheta(t)' + \frac{1}{\tau} \vartheta(t) = \frac{W}{mc_p} + \frac{1}{\tau} \vartheta_{RT}, \qquad (12)$$

where $(')$ means derivation with respect to time; m is the rivet mass; c_p is the specific heat of the titanium alloy; ϑ is the rivet temperature; W is the thermal power resulting from the thermal analysis equal to q_c calculated through Equation 5 multiplied by A_c that is the contact area between rivet and laminate. τ is the time constant of the system with the following technical meaning: it is the time needed to the system for reaching $(1 - \frac{1}{e})\% \approx 63.2\%$ of its asymptotic or final value. The lower is τ, the faster is the rivet heating.

The hypotheses made on the analytical model are, therefore, the following: the riveted joint is assumed as a lumped parameters body subjected to the heat calculated by the finite element model; the thermal equilibrium condition on the bolt comes from the balance between the applied thermal load, the conduction from the bolt to the rest of the joint, and the convection from the bolt to the air.

The general solution of 12 has the following form:

$$\text{Solution}: \vartheta(t) = Be^{-t/\tau} + \frac{W}{h_f A_s} + \vartheta_{RT}, \qquad (13)$$

$$\text{Initial condition}: \vartheta(0) = \vartheta_{RT}, \qquad (14)$$

$$\text{Boundary condition}: \lim_{t \to \infty} \vartheta(t)' = 0. \qquad (15)$$

The constant B was obtained from the initial condition:

$$B = -\frac{W}{h_f A_s}. \qquad (16)$$

Using the boundary condition, Equation 13 can be written as follows:

$$\vartheta(\infty)' + \frac{1}{\tau} \vartheta(\infty) = \frac{W}{h_f A_s} + \frac{1}{\tau} \vartheta_{RT} \rightarrow \vartheta_{FIN} - \vartheta_{RT} = \frac{W}{h_f A_s}, \qquad (17)$$

$$\vartheta(t) = \vartheta_{RT} + (\vartheta_{FIN} - \vartheta_{RT})\left(1 - e^{-t/\tau}\right), \qquad (18)$$

where ϑ_{FIN} is the temperature after a meaningfully long time.

The experimental evidence and the FE analyses revealed that titanium alloy pins of rivets are subjected to strong increments of temperature during the fatigue tests. Furthermore, the temperature field over them is completely uniform, since titanium alloys are characterized by a high thermal conductivity that makes irrelevant the convection effect. According to the material properties and geometry, the time constant for the rivets was found to be approximately equal to $942\,s$ according to the analytical model. In Figure 8, the numerical results obtained by the FE models are compared with the
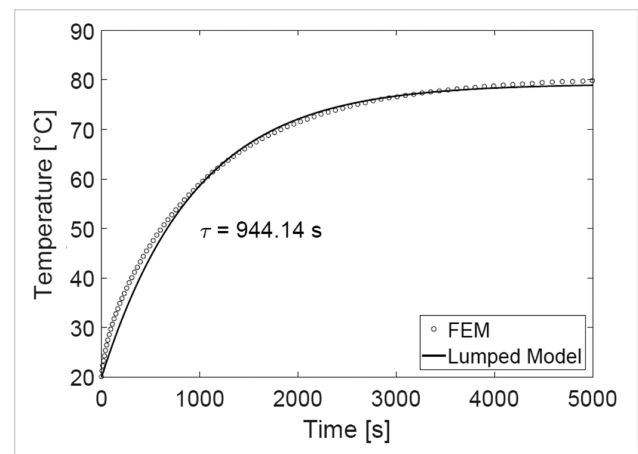
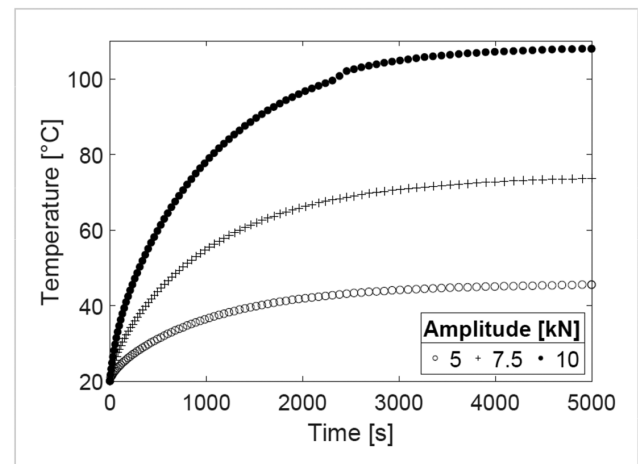**FIGURE 8** Comparison between FE and analytical model

FIGURE 9 Configuration 2, $f = 3.5$ Hz

simplified analytical model for one configuration (Configuration 1 of Table 1) at one test frequency and load level (3.5 Hz, 10 kN). In Figure 9, the numerical FE results for one of the numerically investigated cases are reported.

The following conclusions can be formulated:

1. For all the cases, lumped model and FE model results are in close agreement.
2. Time constant τ provided by the FE simulations assumes values between 906 and 1005 s that is quite close to the value analytically calculated 942 s. As previously demonstrated (see Equations 11 and 12), τ resulted a function of convection surfaces and material properties and not of load parameters: from Equations 11 and 12, it is possible to see that the time constant of the system depends only on material properties (mass, m, and specific heat capacity, c_p), convection areas (A_s), and film convection coefficient (h); thus, the lumped system will reach 63.2% $(1-e^{-1})$ of the final temperature after a time constant independently from load.
3. The final temperature at the rivets increases with increasing load amplitude and frequency: the increase with load amplitude results directly from the Equation 4 in which the shear stress, strictly proportional

to the load amplitude, appears affecting the generated heat flux at the interface between the two laminates. The load frequency increase results in a higher V and this turns in a higher temperature at rivets.

4. The final temperature at the rivets is strongly influenced by the dimension tolerances of holes and rivets that determined the sliding distance. If these tolerances would originate a higher clearance, the sliding distance would increase as far as the temperature. This effect can be explained by the amount of generated heat that, according to the Equation 4, depends on the sliding rate V: a higher sliding distance, at the same load frequency, results in a higher V.
5. The highest temperature was observed for the Configuration 3 with an amplitude load of 10 kN and at 5 Hz. For this case, the rivets reached 109°C after 912 s (equal to a time constant) and after 4562 s (1 h approximately) they were at 99.3% of $\vartheta_F IN$. The lowest temperature (31°C) was observed on Configuration 1 for the case at 2 Hz and 5 kN. These results are in agreement with the experimental tests performed by the authors.[27,28]

4.4 | Comparison between experiments and numerical results

The temperature maps provided by IR camera were post-processed in Matlab, and the maximum temperature on the rivet surface was obtained for each recorded thermal frame. Since a time interval of 120 s between frames was used, the temperature behavior of the rivet was reconstructed and is reported in Figure 10 for one of the three experimental cases of interest.

The correlation between the simulation and the experiments is summarized in Tables 5 and 6. For the experimental Case 1 (Configuration 1 of the specimen, tested at an amplitude load of 10 kN at 3.5 Hz), a time constant of about 922 s was found (4.8% and 2.4% smaller than numerical and analytical value, respectively) with a final temperature $\vartheta_F IN$ of 79.0°C.

For Case 2 (Configuration 2, tested by a load amplitude of 7.5 kN at 5 Hz), a time constant of 891 s was found with a temperature increment of 72°C
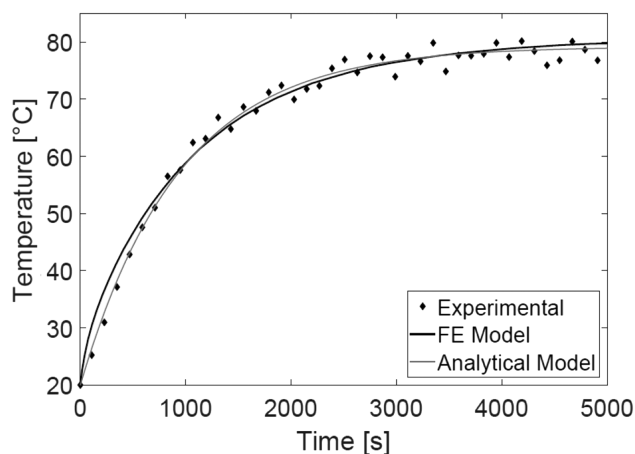

FIGURE 10 Configuration 1, frequency = 3.5 Hz, amplitude = 10 kN

TABLE 5 Comparison between analytical, numerical and experimental results

	Frequency (Hz)	Amplitude (kN)	τ (s)			ϑ_{FIN} (°C)		
			Analytical	FE	Exp	Analytical	FE	Exp
Case 1	3.5	10.0	944.1	966.9	922.0	79.8	79.2	79.0
Case 2	5.0	7.5	915.7	1005.0	891.0	94.0	92.9	92.0
Case 3	5.0	5.0	971.1	947.7	932.7	58.4	57.9	55.5

	Mean (°C)		Maximum (°C)		$\tau - PAE$ (%)		$\vartheta_{FIN} - PAE$ (%)	
	Analytical	FE	Analytical	FE	Analytical	FE	Analytical	FE
Case 1	3.8	4.1	4.6	4.1	2.4	4.8	1.0	0.2
Case 2	1.7	2.5	4.5	6.1	2.7	12.0	2.0	0.9
Case 3	2.4	2.5	5.7	6.0	4.1	1.6	5.2	4.3

TABLE 6 Mean, maximum absolute error on the instantaneous temperature, and percent absolute error (PAE) of analytical and FE models, with respect to the experiments

($\vartheta_F IN = 92°C$). For this case, the highest difference in terms of time constant between experimental case and FE model was found: 63.2% of $\vartheta_F IN$ was reached after only $891\,s$ during the experiment, while the thermal response of numerical model was slower exhibiting a time constant of $1005\,s$.

For Case 3 (Configuration 3, with a load amplitude of $5\,kN$ applied at $5\,Hz$), the difference between numerical and experimental time constants is only $15\,s$ and the values of the final temperatures are quite similar.

However, the agreement of the three experimental tests with the prediction of the numerical and analytical models is generally good, confirming the validity of the proposed models.

5 | CONCLUSIONS

Fatigue response is a complex phenomenon that involves aspects that are generally neglected in static tests. The influence of load ratio is considerably evident if the applied load allows recuperating clearance existing between holes and fastener as in the carried out analyses in which a $R = -1$ was used. Cyclic loads, in the presence of joints for which the tolerance of the holes is not properly controlled, can cause significant temperature increases due to friction phenomena between laminates. This effect that is particularly pronounced at higher frequencies and load amplitudes was simulated in the present work by a complex thermomechanical numerical model following a step by step procedure taking into account the different physical parameters involved in the heat generation: this numerical procedure represents the main novelty of this work and a proper use of this allows to draw design criteria for structural bolted joints operating under different conditions (single and double joints, static and dynamic conditions, different preloads, and so on). Another important conclusion is that a riveted joint can be described analytically by a simple first-order system, after the thermal loads are provided numerically. The finite element analyses highlighted the importance of evaluating the temperature field in the region between fasteners in order to avoid situation in which laminates work at temperature higher than those allowed by polymeric matrix.

ORCID

Gennaro Scarselli https://orcid.org/0000-0002-8652-2998

REFERENCES

1. Camanho PP, Matthews FL. Stress analysis and strength prediction of mechanically fastened joints in FRP: a review. *Compos Part a - Appl S.* 1997;28(6):529-547.
2. Thoppul SD, Finegan J, Gibson RF. Mechanics of mechanically fastened joints in polymer–matrix composite structures—a review. *Compos Sci Technol.* 2009;69(3–4):301-329.
3. Schön J, Nyman T. Spectrum fatigue of composite bolted joints. *Int J Fatigue.* 2002;24(2–4):273-279.
4. Zhang KD, Ueng CE. Stresses around a pin-loaded hole in orthotropic plates. *J Compos Mater.* 1984;18(5):432-446.
5. Hyer MW, Klang EC. Contact stresses in pin-loaded orthotropic plates. *Int J Solids Struct.* 1985;21(9):957-975.
6. Gamdani F, Boukhili R, Vadean A. Tensile strength of open-hole, pin-loaded and multi-bolted single-lap joints in woven composite plates. *Mater Design.* 2015;88:702-712.
7. Wu T, Zhang K, Cheng H, Liu P, Song D, Li Y. Analytical modeling for stress distribution around interference fit holes on pinned composite plates under tensile load. *Compos Part B - Eng.* 2016;100:176-185.
8. Van Der Sypt P, Chérif M, Bois C. Analysis of the fatigue behaviour of laminated composite holes subjected to pin-bearing loads. *Int J Fatigue.* 2017;103:86-98.
9. Zou P, Zhang K, Li Y, Liu P, Xie H. Bearing strength and failure analysis on the interference-fit double shear-lap pin-loaded composite. *Int J Damage Mech.* 2018;27(2):179-200.
10. Sobotka JC, McClung RC. Modelling considerations for stress intensity factor solutions at pin-loaded holes. *Fatigue Fract Eng M.* 2020;43(5):955-964.
11. Hajimohamadi M, Ghajar R. Stress intensity factors for cracks emanating from a circular hole in an infinite quasi-orthotropic plane. *Fatigue Fract Eng M.* 2019;42(3):743-751.
12. Liu N, Cui X, Xiao J, Lua J, Phan N. A simplified continuum damage mechanics based modeling strategy for cumulative fatigue damage assessment of metallic bolted joints. *Int J Fatigue.* 2020;131:105302.
13. ASTM. D5961/D5961M-13, Standard test method for bearing response of polymer matrix composite laminates, Am. Soc. Test. Mater. (2013). https://doi.org/10.1520/D5961

14. D7248/D7248M-07, Standard Test Method for Bearing/Bypass Interaction Response of Polymer Matrix Composite Laminates Using 2-Fastener Specimens, in: ASTM B. Stand., 2008. https://doi.org/10.1520/D7248_D7248M-12

15. D6873/D6873M-08, Standard Practice for Bearing Fatigue REsponse of Polymer Matrix Composite Laminates, in: ASTM B. Stand., 2017. https://doi.org/10.1520/C0305-14.2

16. Tserpes KI, Papanikos P, Kermanidis TH. A three-dimensional progressive damage model for bolted joints in composite laminates subjected to tensile loading. *Fatigue Fract Eng M*. 2001;24 (10):663-675.

17. Saunders DS, Galea SC, Deirmendjian GK. The development of fatigue damage around fastener holes in thick graphite/epoxy composite laminates. *Composites*. 1993;24(4):309-321.

18. Chakherlou TN, Abazadeh B. Estimation of fatigue life for plates including pre-treated fastener holes using different multiaxial fatigue criteria. *Int J Fatigue*. 2011;33(3):343-353.

19. Whitworth HA. Fatigue evaluation of composite bolted and bonded joints. *J Adv Mater*. 1998;30(2):25-31.

20. Smith PA, Pascoe KJ. Fatigue of bolted joints in (0/90) CFRP laminates. *Compos Sci Technol*. 1987;29(1):45-69.

21. Giannopoulos IK, Doroni-Dawes D, Kourousis KI, Yasaee M. Effects of bolt torque tightening on the strength and fatigue life of airframe FRP laminate bolted joints. *Compos Part B - Eng*. 2017;125:19-26.

22. Starikov R, Schön J. Experimental study on fatigue resistance of composite joints with protruding-head bolts. *Compos Struct*. 2002;55(1):1-11.

23. Counts WA, Johnson WS. Bolt bearing fatigue of polymer matrix composites at elevated temperature. *Int J Fatigue*. 2002; 24(2–4):197-204.

24. Kapidžić Z, Ansell H, Schön J, Simonsson K. Fatigue bearing failure of CFRP composite in bolted joints exposed to biaxial variable amplitude loading at elevated temperature. *Compos Struct*. 2016;142:71-77.

25. Kapidžić Z, Ansell H, Schön J, Simonsson K. Fatigue bearing failure of CFRP composite in biaxially loaded bolted joints at elevated temperature. *Compos Struct*. 2015;127:298-307.

26. Sauer JA, Richardson GC. Fatigue of polymers. *Int J Fracture*. 1980;16(6):499-532.

27. Dattoma V, Nobile R, Scarselli G, Panella FW. Fatigue testing of CFRP aeronautical laminates for bearing behaviour characterisation. In 9th International Conference on Composite Science and Technology, 24–26 April 2013, Sorrento, Italy, 275-283.

28. Scarselli G, Castorini E, Panella FW, Nobile R, Maffezzoli A. Structural behaviour modelling of bolted joints in composite laminates subjected to cyclic loading. *Aerosp Sci Technol*. 2015; 43:89-95.

29. Thompson MK, Thompson JM. *ANSYS Mechanical APDL for Finite Element Analysis*. Butterworth-Heinemann; 2017.

30. Montgomery J. Methods for modeling bolts in the bolted joint. In ANSYS User's Conference 2002 Apr (Vol. 5).

31. Alawadhi EM. *Finite Element Simulations Using ANSYS*. CRC Press; 2015.

32. Miltenović A, Banić M, Stamenković D, Milošević M, Tomić M. Determination of friction heat generation in wheel-rail contact using FEM. *Facta Universitatis, Series: Mechanical Engineering*. 2015;13(2):99-108.

33. Bergman T, Incropera F. *Introduction to Heat Transfer*. John Wiley & Sons; 2011.